

APPLIED SCIENCES AND ENGINEERING

Soft artificial electroreceptors for noncontact spatial perception

Won Jun Song^{1†}, Younhoon Lee^{1†}, Yeonsu Jung^{2,3†‡}, Yong-Woo Kang¹, Junhyung Kim², Jae-Man Park¹, Yong-Lae Park², Ho-Young Kim^{2*}, Jeong-Yun Sun^{1,4*}

Elasmobranch fishes, such as sharks, skates, and rays, use a network of electroreceptors distributed on their skin to locate adjacent prey. The receptors can detect the electric field generated by the biomechanical activity of the prey. By comparing the intensity of the electric fields sensed by each receptor in the network, the animals can perceive the relative positions of the prey without making physical contact. Inspired by this capacity for prey localization, we developed a soft artificial electroreceptor that can detect the relative positions of nearby objects in a noncontact manner by sensing the electric fields that originate from the objects. By wearing the artificial receptor, one can immediately receive spatial information of a nearby object via auditory signals. The soft artificial electroreceptor is expected to expand the ways we can perceive space by providing a sensory modality that did not evolve naturally in human beings.

INTRODUCTION

Human beings recognize the relative positions of surrounding objects using their visual, tactile, and auditory sensory abilities (1). Visual sensation based on binocular disparity plays an especially vital role in spatial perception (2). The distance of a few centimeters between a person's two eyes means that each retina generates a different two-dimensional image; the brain then recognizes the relative positions of objects by comparing the two images. However, people who are blind or visually impaired cannot rely on visual sensation to perceive space. They have to depend on tactile sensation to recognize surrounding objects, which can lead to injuries by causing unwanted contact with dangerous objects. Thus, artificial sensory systems that can support spatial perception in daily life are needed.

Some animals have successfully evolved sensory modalities that have not evolved naturally in human beings. For example, elasmobranch fishes, such as sharks, skates, and rays, depend on a network of electroreceptors distributed on their skin to locate nearby prey without making physical contact (Fig. 1, A and B) (3–5). Each electroreceptor, which can be deformed smoothly along with the skin, has two components (Fig. 1C) (5, 6). An ion-conducting hydrogel core acts as a soft electric field receiver that receives the electric field generated by the biomechanical activity of prey animals, and an ion-insulating epithelium surrounding the hydrogel acts as a soft encapsulation layer. Although an individual electroreceptor can only sense the intensity and polarity of the electric field, the animals can perceive the relative positions of nearby prey without making physical contact by comparing the intensity of the electric fields sensed by each electroreceptor in the network (5, 6).

¹Department of Materials Science and Engineering, Seoul National University, 1 Gwanak-ro, Gwanak-gu, Seoul 08826, South Korea. ²Department of Mechanical Engineering, Seoul National University, 1 Gwanak-ro, Gwanak-gu, Seoul 08826, South Korea. ³School of Engineering and Applied Sciences, Harvard University, Cambridge, MA 02138, USA. ⁴Research Institute of Advanced Materials (RIAM), Seoul National University, 1 Gwanak-ro, Gwanak-gu, Seoul 08826, South Korea.

*Corresponding author. Email: hyk@snu.ac.kr (H.-Y.K.); jysun@snu.ac.kr (J.-Y.S.)

†These authors contributed equally to this work.

‡Present address: School of Engineering and Applied Sciences, Harvard University, Cambridge, MA 02138, USA.

Inspired by this sensory mechanism, we introduce a soft artificial electroreceptor (SAER) for noncontact spatial perception (Fig. 1, D and E). As in the electroreceptors found in elasmobranch fishes, ionic conductive hydrogels were used as the soft electric field receivers of the SAER (Fig. 1F). On the basis of electrostatic induction, these receptors can detect the electric field that originates from the object's static charge. By comparing the intensity of electric fields sensed by each hydrogel receiver, the relative position of the nearby object can be estimated in the same manner as by the animals. Because an electric field can be transmitted through dielectric materials, a SAER can be used to detect objects behind a dielectric wall.

RESULTS

Electroreception in rays for noncontact prey localization

Using network of electroreceptors distributed in the skin around the mouth and gills, ocellate river stingrays (i.e., *Potamotrygon motoro*) can sense the electric fields generated by the biomechanical activity of prey animals within a few centimeters (Fig. 2A) (7, 8). By comparing the intensities of the electric fields sensed by each electroreceptor in the network, the rays can identify the relative positions of nearby prey.

To experimentally characterize electroreception in rays, two electrodes and an odor-delivery tube were placed on the bottom of a tank and covered with sand (see Fig. 2B, Materials and Methods, and movie S1 for details) (4). Initially, the ray was in a resting state and showed little movement. To elicit the prey-searching behavior of the ray, a food odor was injected into the center of the tank via the odor-delivery tube. When the ray detected the odor, it began to actively swim to find a prey (Fig. 2C). However, because both electrodes were turned off, the prey-searching behavior was not biased toward a specific direction (Fig. 2D). In contrast, when prey-simulating electric fields were generated via the left electrode, the ray hovered around the electrode trying to find prey (Fig. 2E) (7). The ray stayed 44 times longer near the left electrode than it did near the right electrode (Fig. 2F). This indicates that electroreception has potential for noncontact spatial perception.

Copyright © 2021
The Authors, some
rights reserved;
exclusive licensee
American Association
for the Advancement
of Science. No claim to
original U.S. Government
Works. Distributed
under a Creative
Commons Attribution
NonCommercial
License 4.0 (CC BY-NC).

Downloaded from https://www.science.org at Seoul National University Library on November 27, 2021

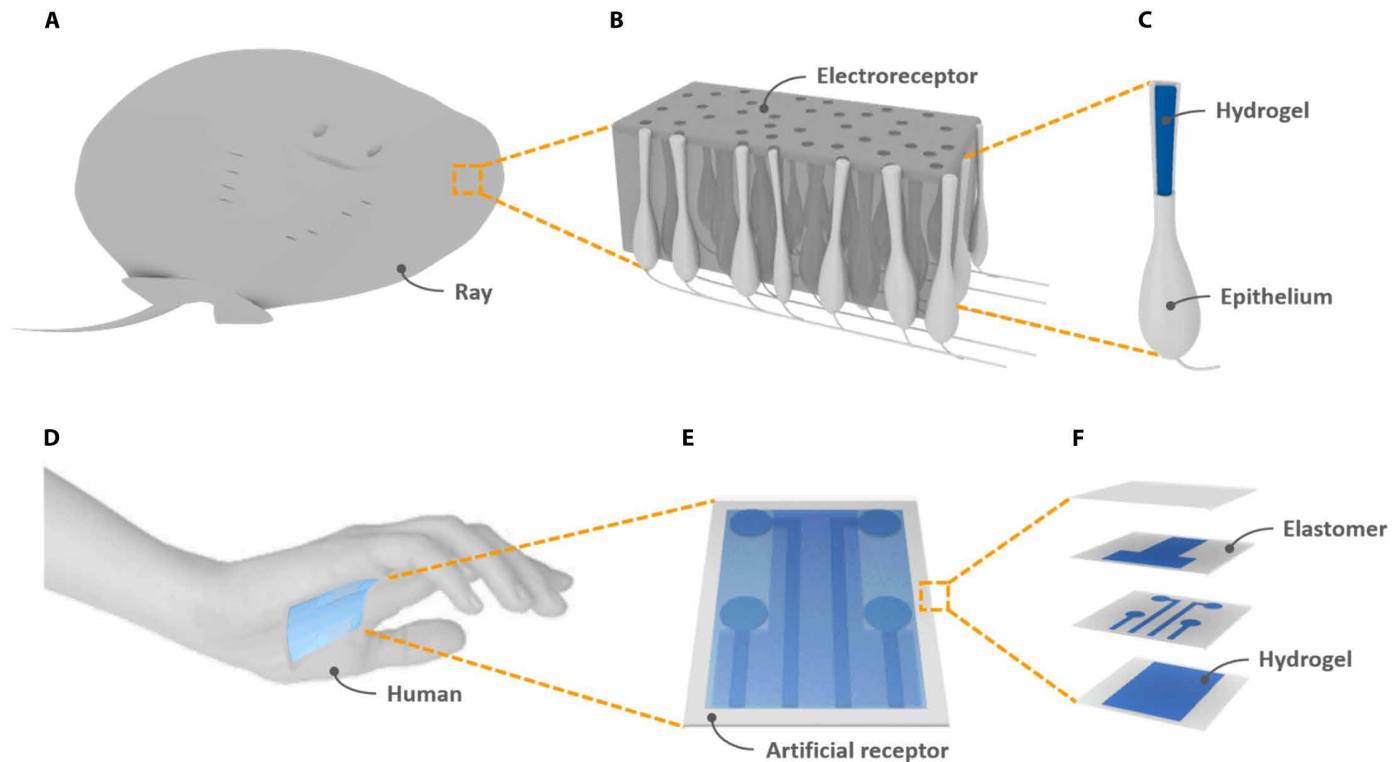


Fig. 1. A soft artificial electroreceptor (SAER). (A and B) Rays use a network of electroreceptors distributed on their skin to locate nearby prey. (C) Each receptor, consisting of an ionic conductive hydrogel-filled canal, can detect the electric field generated by the biomechanical activity of prey animals. By comparing the intensity of the electric fields sensed by each receptor in the network, rays can estimate the relative position of nearby prey without making physical contact. (D) A wearable SAER was developed to support human spatial perception in daily life. (E and F) Same as the ray, the SAER can locate the relative positions of nearby objects by comparing the intensity of the electric fields sensed by each hydrogel electric field receiver.

Fabrication of a SAER with high mechanical reliability

Highly compliant electroreceptors found in elasmobranch fishes inspired us to build a SAER consisting of soft conductors and insulators. This facilitated a comfortable interface between the artificial receptor and human beings (9–11). On the basis of their high ionic conductivity and stretchability, hydrogels are promising materials as soft conductors for the SAER (12–20). Moreover, elastomers are suitable for use as soft insulators because they can effectively block the migration of mobile ions in a hydrogel without deteriorating the hydrogel's stretchability (21–24). However, because of low surface energy of elastomers, their poor adhesion with hydrogels can lead to the interface delamination under mechanical deformation, thus limiting the wearable applications of the SAER (12, 13, 25). This issue becomes especially critical when three-dimensional (3D) printing technology is used to print a hydrogel directly on an elastomer for rapid and high-resolution fabrication. Although there have been considerable efforts to adhere hydrogels with elastomers (25–29), it remains challenging to form a robust interface between the two during 3D printing to secure mechanical reliability.

To fabricate a mechanically reliable SAER using 3D printing technology, we covalently anchored hydrogels to elastomers during the printing process (see Fig. 3A and the Supplementary Materials for details). First, a preshaped elastomer was immersed in a solution with an ultraviolet (UV)-assisted grafting agent for swelling-driven absorption (Fig. 3A, i). The grafting agent absorbed elastomer was treated with 365-nm UV light for 10 s to promote radical formation

at polymer chains (Fig. 3A, ii). Then, the hydrogel was directly printed on the UV-treated elastomer using a digital light processing (DLP) 3D printer (Fig. 3A, iii). During the printing process, radicals of the elastomer participate in free-radical polymerization of the hydrogel, thus forming a covalently cross-linked robust interface (Fig. 3, B and C, and fig. S1). Last, the SAER was assembled by stacking the printed layers (Fig. 3A, iv).

From grafting agent activation to printing, the overall time required to fabricate each layer of the SAER is less than 1 min (see Materials and Methods for details). Furthermore, the maximum resolution of the printed hydrogel is 50 μm , which is sufficient to print the hydrogel network of the SAER (Fig. 3C). Although the hydrogel/elastomer interface can be translucent during the covalent cross-linking process (22), the fabricated SAER is as transparent as the individual elastomer and hydrogel because the rapidly fabricated hydrogel/elastomer interface scatters a negligible amount of visible light (Fig. 3D). Moreover, the robust interface can withstand a mechanical strain of more than 300% without delamination, allowing the SAER to be used in wearable applications (Fig. 3E and movie S2).

Sensing capability of the SAER

On the basis of electrostatic induction, the SAER can sense an electric field originating from static charges on the surface of an object. Because contact with its surroundings causes the object to be charged through contact electrification, objects usually have static charges on their surfaces (Fig. 4A) (21, 22, 30–32). When an object

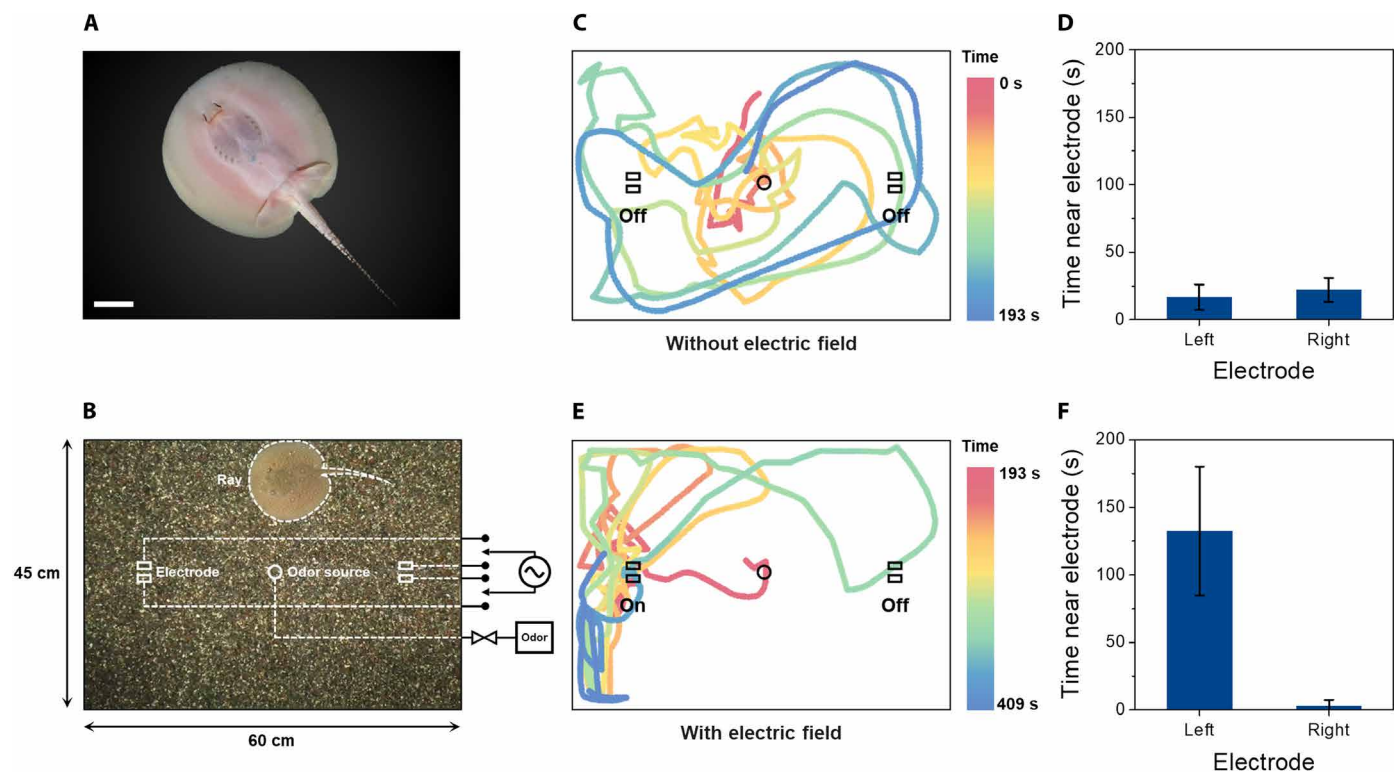


Fig. 2. Electrorception in rays for noncontact prey localization. (A) Electroreceptors of an ocellate river stingrays (i.e., *P. motoro*) distributed in the skin around the mouth and gills. Scale bar, 3 cm. (B) The experimental setup used to characterize electroreception in the ray. Two electrodes and an odor-delivery tube were buried under the sand. (C) Swimming trajectory of the ray when a food odor was injected into the center of the tank via the odor-delivery tube. The ray randomly swam in an attempt to find prey. (D) The time that the ray spent within 7.5 cm from each electrode. The prey-searching behavior of the ray was not biased toward a specific direction. (E) When prey-simulating electric fields were generated via the left electrode, the ray hovers around the electrode in an attempt to find prey. (F) The ray stayed 44 times longer near the left electrode than the right electrode. Error bars represent SD ($n = 5$). Photo credit: Won Jun Song and Younghoon Lee, Seoul National University.

is approaching the receptor, electric fields originating from the object gradually increase the induced voltage in the hydrogel electric field receiver of the SAER (Fig. 4B). This causes an electric current and potential drop across the external load between the receiver and ground. Thus, by measuring the induced voltage across the external load, one can estimate the intensity and polarity of the object's electric field that reaches the receiver. To investigate voltage induction as a function of distance between the object and the receiver, the finite element method (FEM) was used (Fig. 4C). As the object approaches the receptor, the intensity of the object's electric field reaches the receiver increases, and higher voltage is induced across the external load. Thus, the object's approach can be sensed by measuring the induced voltage.

To consolidate the sensing mechanism of the SAER, theoretical analysis was carried out (see the Supplementary Materials for details). As shown in Fig. 4D, the electric field receiver of the SAER and the object can be represented by two separated parallel plates. The top plate, which is connected to a constant voltage source of voltage V_0 , represents the charged object. The bottom plate, which is connected to the external load of electrical resistance R , represents the receiver of the SAER. To measure the induced voltage across the external load, V , a voltage meter is connected in parallel to the external load. The total electric charge on the receiver of the SAER, q , is linearly proportional to the potential difference between the object and the receiver, following $q = -C(V_0 - V)$, where C is the

capacitance between the object and the receiver. Moreover, the object-SAER system obeys Ohm's law, $dq/dt = -V/R$, where the electric current from the receiver to the external load is set as a positive value. By combining the two equations, an ordinary differential equation that governs the object-SAER system can be obtained, which is written as

$$\frac{dq}{dt} = -\frac{q}{RC} - \frac{V_0}{R} \quad (1)$$

with the initial condition $C_0 = C(t = 0)$ and $q(t = 0) = -C_0V_0$. Thus, $V(t)$ can be obtained from the exact solution of Eq. 1, which can be written as

$$V(t) = V_0 \left\{ 1 - \frac{p(t)}{\mu(t)} \left[\int_0^t \mu(t') dt' + 1 \right] \right\} \quad (2)$$

where $p(t) = C_0/C(t)$ and $\mu(t) = \exp \left[\int_0^t p(t') dt' \right]$. Although Eq. 2 enables a comparison between theoretical and experimental results, it would be more intuitive if an approximate expression for the induced voltage could be obtained by harnessing the Fourier transform of Eq. 1. For this approximation, the movement of the object is represented by vertical simple harmonic oscillations. Thus, the distance between the object and the receiver, d , follows $d = d_i + d_a \sin(2\pi ft)$, where f is the oscillation frequency, d_i is the initial distance,

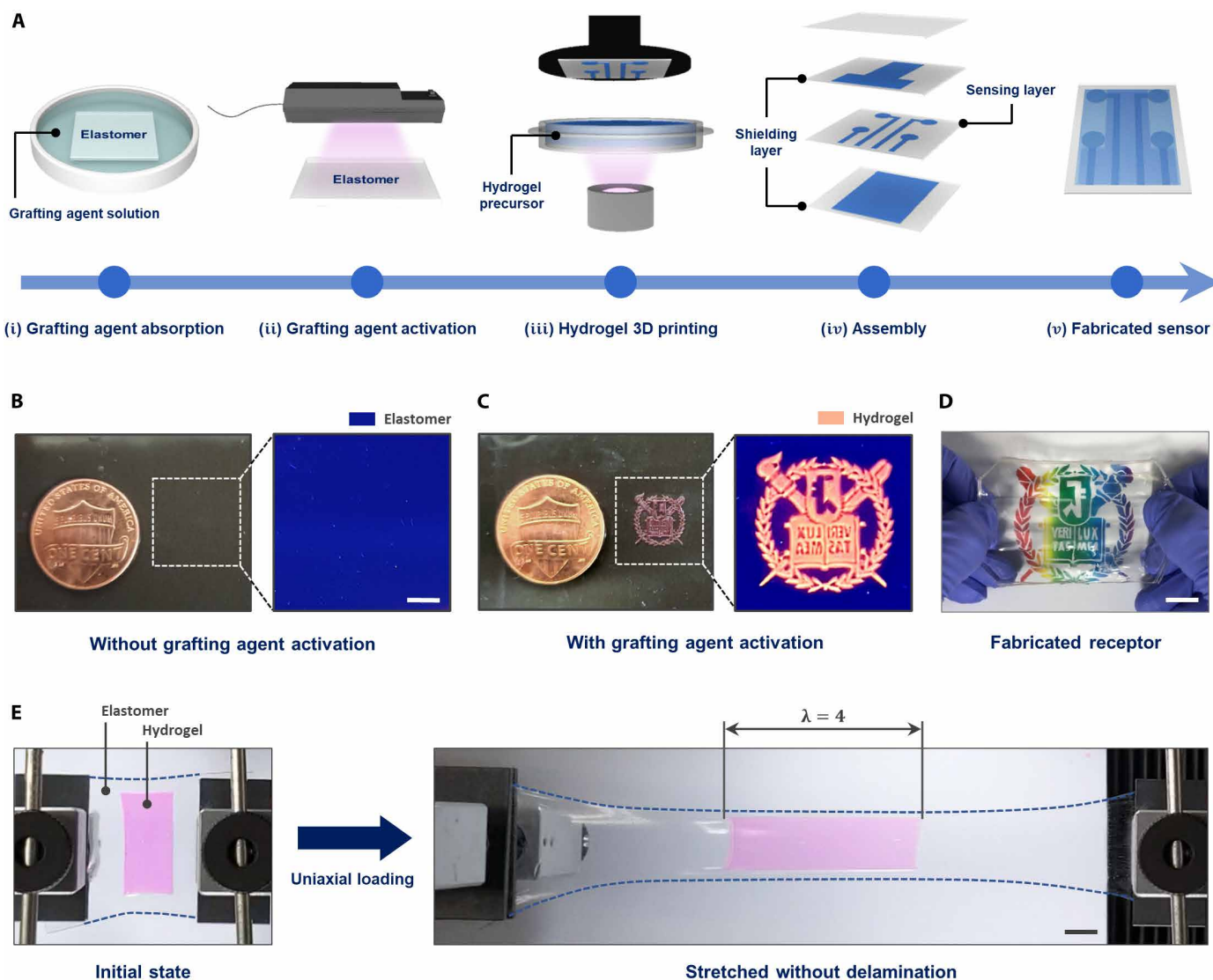


Fig. 3. Fabrication of a SAER with high mechanical reliability. (A) Conductive hydrogels were covalently anchored to an elastomer during 3D printing for rapid and elaborate fabrication of a SAER with high mechanical reliability. (B) In the absence of grafting agent activation, delamination occurs between the hydrogels and the elastomer during the printing process due to poor interfacial bonding. Scale bar, 250 μm . (C) Grafting agent activation allows radicals in the elastomer to participate in free-radical polymerization of the hydrogel during printing, thus forming a tough interface between the hydrogel and elastomer layers. To enhance the contrast between the hydrogel and elastomer, fluorescent dyes were added to the hydrogel. (D) The SAER was highly transparent to visible light of all colors because the rapidly fabricated hydrogel/elastomer interface scatters a negligible amount of visible light. Scale bar, 1 cm. (E) The hydrogel layer on the elastomer could be stretched more than 400% without delamination. To enhance the contrast between the hydrogel and elastomer, fluorescent dyes were added to the hydrogel. Scale bar, 1 cm. Photo credit: Won Jun Song and Younghoon Lee, Seoul National University.

and d_a is the oscillation amplitude. The Fourier transform of $q(t)$, $\mathcal{F}[q(t)]$, is written as

$$\hat{q}(\omega) = \mathcal{F}[q(t)] = \frac{1}{\sqrt{2\pi}} \int_{-\infty}^{\infty} q(t) \exp(-i\omega t) dt \quad (3)$$

where $\mathcal{F}[q'(t)] = i\omega\hat{q}(\omega)$. The Fourier transform of Eq. 1 yields a functional relationship between $\hat{q}(\omega)$ and $\hat{p}(\omega) = \mathcal{F}[p(t)]$, which is given by

$$i\omega\hat{q}(\omega) = \frac{1}{\sqrt{2\pi}} f_c \hat{p}(\omega) * \hat{q}(\omega) - \frac{\sqrt{2\pi} V_0}{R} \delta(\omega) \quad (4)$$

where δ is the Dirac delta function and “*” denotes the convolution operation. Given that $p(t)$ is an oscillating function predominantly composed of two frequency components that are null and $\omega_0 = 2\pi f$, $\hat{p}(\omega)$ can be assumed to be $\hat{p}(\omega) \sim \delta(\omega) + \delta(\omega - \omega_0)$, which leads to the expression of amplitude of $\hat{V}(\omega) = \mathcal{F}[V(t)]$ at $\omega = \omega_0$

$$\hat{V}(\omega_0) \sim \frac{\omega_0^2}{\omega_0^2 + \left(\frac{1}{RC_0}\right)^2} V_0 \quad (5)$$

where $V_0 \sim \hat{q}(0)/C_0$. According to Eq. 5, if $\omega_0 \gg 1/(RC_0)$ or $R \gg 1/(2\pi f C_0)$, then $\hat{V}(\omega_0)$ asymptotes to its maximum value and becomes

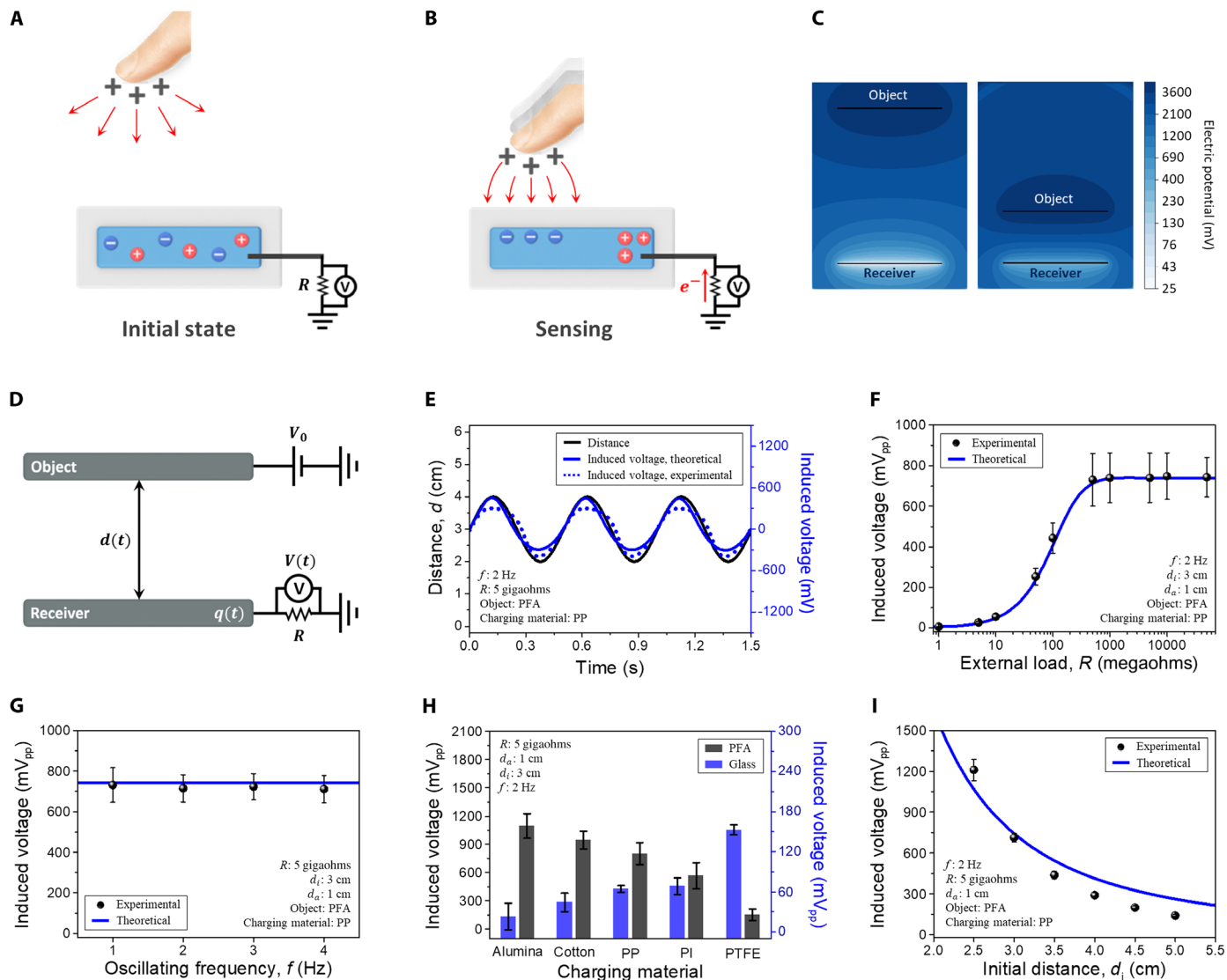


Fig. 4. Sensing capability of the SAER. (A and B) Schematic diagrams illustrating the sensing mechanism of the SAER. Objects usually have static charges on their surfaces because contact with its surroundings causes the object to be charged through contact electrification (A). The electric fields originating from the object induce voltage in the hydrogel electric field receiver of the SAER (B). By measuring the voltage across the external load connected between the receiver and ground, the intensity and polarity of the electric field can be estimated. (C) The finite element method (FEM) was used to investigate voltage induction as a function of distance between the object and the receiver. (D) Equivalent circuit of the object-SAER system for theoretical analysis. (E) The induced voltage closely traced the position of the object. (F to I), The induced voltage was measured while varying the external load resistance (F), oscillating frequency of the object (G), object and charging materials (H), and initial distance between the SAER and the object (I). Error bars represent SD ($n = 3$). PP, polypropylene; PI, polyimide; PTFE, polytetrafluoroethylene.

insensitive to f . This indicates that, by greatly increasing the resistance of the external load, the SAER can more sensitively detect object movement, without being affected by the relative speed between the object and the receptor.

To experimentally characterize the sensing capability of the SAER, a charged object was fixed to a pushing tester that provided consistent vertical simple harmonic oscillation (see Materials and Methods and fig. S2 for details). To compare theory and experiment, Eqs. 2 and 5 were used with $V_0 = -4.706$ V and $C = 1052C_{FEM}$, where C_{FEM} stands for the capacitance between the object and the receiver calculated using FEM (see the Supplementary Materials and fig. S3 for details). When the pushing tester generated vertical

oscillation of the object, the induced voltage closely traced the relative position of the object with various amplitudes (Fig. 4E and fig. S4). This finding reveals the outstanding potential of the SAER to detect the movement of nearby objects in a noncontact manner. To verify the theoretical prediction of Eq. 5, the induced voltage was measured as the resistance of the external load was varied. When the resistance of the external load increased from 1 megohm to 50 gigohm, the induced voltage increased by more than 130-fold, following the theoretically predicted curve as shown in Fig. 4F. The induced voltage rapidly increases near $R = 100$ megohm and asymptotes to its maximum value as described in Eq. 5. This indicates that the sensitivity of the SAER can be maximized by greatly increasing

the resistance of the external load. Moreover, when the resistance of the external load was extremely high, the sensing capability of the SAER was barely affected by the relative speed between the object and the receptor, as predicted by Eq. 5 (Fig. 4G). The induced voltage remained stable around 720 mV_{pp} even when the oscillation frequency of the object was increased fourfold.

To investigate the effect of object surface charge on the sensing capability of the SAER, perfluoroalkoxy alkane (PFA) and glass were charged by rubbing against various materials including alumina, cotton, polypropylene (PP), polyimide, and polytetrafluoroethylene (Fig. 4H). As the difference in electron affinity between the charging materials and the object increased (fig. S5), the density of the object surface charge increased, and a higher voltage was induced across the external load. Meanwhile, although the electron affinity of glass and alumina are quite similar, perceptible values of 23 mV_{pp} were still observed when the glass object was charged with alumina (21). This indicates that objects in the vicinity can be sensed using the SAER as long as they are charged. In addition, the receptor can more sensitively detect an object's movement when that object is close to the SAER (Fig. 4I). This is because the intensity of the electric field reaching the receptor increases as the distance between the object and the SAER decreases.

The resistivity of the hydrogel varies based on its composition (12–14). Thus, to experimentally characterize the effect of the electric field receiver's resistance on the sensing capability of the SAER, the induced voltage was measured using a hydrogel electric field receiver with various ion concentrations and water contents. When the lithium chloride (LiCl) concentration decreased from 2 M to 2 mM, the sensing capability of the SAER was barely diminished (fig. S6). Moreover, the induced voltage remained stable around 720 mV_{pp}, even when the weight of the hydrogel electric field receiver decreased by more than 42% through water evaporation (see Materials and Methods and fig. S7 for details). This is because the resistance of the external load is several orders of magnitude greater than that of the hydrogel electric field receiver with varying compositions.

Through-wall sensing capability of the SAER

Under an external electric field, a dielectric material becomes polarized and transmits the electric field (33). Thus, even if the object is behind a dielectric barrier, the SAER can still detect object movement (Fig. 5A). Moreover, because the relative permittivity of the dielectric barrier is higher than that of air, the barrier can act as an effective medium to transmit the electric field. Therefore, when a barrier is placed between the SAER and the object, the intensity of the object's electric field reaching the receptor becomes higher.

A theoretical analysis was conducted to quantitatively assess the through-wall sensing mechanism of the SAER (see the Supplementary Materials and fig. S8 for details). When a dielectric material of thickness t_b and relative permittivity ϵ_r is inserted between two parallel plates that were originally separated by a distance d , the original capacitance between the plates $C(d)$ becomes approximately $C(d - t_b + t_b/\epsilon_r)$ if we simply assume that electric fields in the barrier are reduced by a factor of $1/\epsilon_r$ compared to those without barrier (34). Thus, Eq. 2 was used with the modified capacitance to compare theory and experiment.

To experimentally investigate the through-wall sensing capability of the SAER, barriers with various thicknesses and relative permittivity were placed between the object and the receptor. When the

thickness of the glass barrier increased from 2.7 to 16.4 mm, the induced voltage increased from 606.7 to 2003.3 mV following the theoretically predicted curve (Fig. 5B). Moreover, the induced voltage increased by 32.5% when the relative permittivity of the 15-mm-thick barrier increased from 2.1 to 4.6 (see Fig. 5C, Materials and Methods, and table S1 for details). Meanwhile, the static electric field originating from the barrier's surface charges does not affect object detection because a voltage is induced only by the alternating electric field (see the Supplementary Materials and figs. S9 and S10 for details).

Although the electric field can be transmitted through a dielectric material, it cannot be transmitted through a grounded conductor. When the external electric field is applied, excess charges accumulate on the surface of the grounded conductor, preventing transmission of the electric field (Fig. 5D). Thus, the grounded conductor can be used as an effective electric field shield that can prevent unwanted electric fields from reaching the SAER. To characterize the shielding capability of the grounded conductor, hydrogels with various thicknesses and LiCl concentrations were placed between the object and the SAER. More than 99% of the electric field was blocked by the hydrogel conductive shield regardless of hydrogel thickness (Fig. 5E). Even when the hydrogel conductive shield was only 200 μm thick, the induced voltage decreased from 776.6 to 1.3 mV. In addition, the shielding capability of the grounded hydrogel was barely diminished even when the LiCl concentration decreased from 2 M to 2 mM (Fig. 5F).

To demonstrate the through-wall sensing capability, the SAER with two electric field receivers was placed in front of an oscillating pendulum (Fig. 5G). When the induced voltage exceeded a threshold voltage due to the approaching pendulum, the connected computer lit up light-emitting diodes (LEDs) corresponding to the receiver (fig. S11A and movie S3). Moreover, because the electric field can be transmitted through dielectric materials, the SAER could be used to detect the movement of the pendulum even when a barrier was placed between the SAER and the pendulum (Fig. 5H, fig. S11B, and movie S3). When the electric field originating from the pendulum was transmitted through a 2-mm-thick piece of paper and induced a voltage that exceeded the threshold voltage of 5 V, a green LED was turned on, indicating the presence of the pendulum. In contrast, when a 2-mm-thick grounded aluminum sheet was placed between the SAER and the pendulum, the electric fields that originated from the pendulum were blocked by excess charges on the aluminum surface (Fig. 5I, fig. S11C, and movie S3). Thus, a voltage far below the threshold voltage was induced across the external load, and the LED remained off.

Human skin and clothes can be charged through contacting to each other, which result in generating electric fields. Thus, SAER can detect human movements in real time. As shown in Fig. 5J, fig. S12, and movies S4 and S5, SAER can detect the approaching and receding of a person who is walking from meters away. Furthermore, even when a 3-cm-thick wooden wall is blocking between the person and a hydrogel electric field receiver, the SAER successfully detects the movement of a person in real time (see Fig. 5K, Materials and Methods, and movie S4 for details).

A wearable SAER for noncontact spatial perception

Each individual electroreceptor of an elasmobranch fish can only sense the intensity and polarity of the electric field. Thus, elasmobranch fishes depend on a network of electroreceptors to perceive

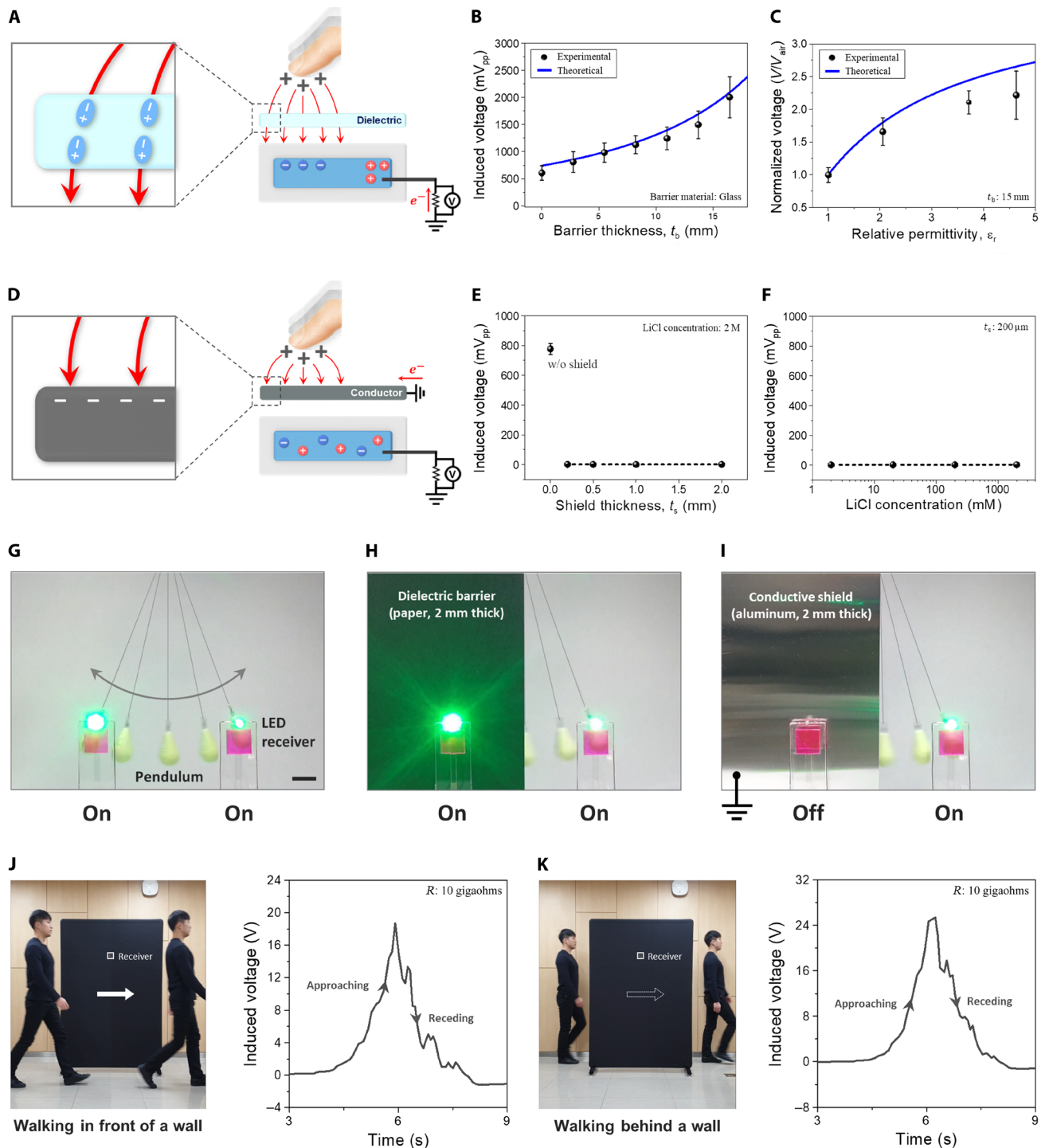


Fig. 5. Through-wall sensing capability of the SAER. (A) Under an external electric field, a dielectric material becomes polarized and transmits the electric field. (B and C) The induced voltage was measured as the thickness (B) and relative permittivity (C) of the dielectric barrier were varied. (D) When an external electric field is applied, excess charges accumulate on the surface of a grounded conductor, preventing transmission of the electric field. (E and F) The induced voltage was measured as the thickness (E) and lithium chloride (LiCl) concentration (F) of the hydrogel conductive shield were varied. (G) A SAER with two hydrogel electric field receivers was placed in front of an oscillating pendulum. Light-emitting diodes (LEDs) were programmed to be turned on when the induced voltage exceeded a threshold voltage. Scale bar, 4 cm. (H) A dielectric barrier was placed between the oscillating pendulum and the receiver on the left side. (I) A conductive shield was placed between the oscillating pendulum and the receiver on the left side. To enhance the contrast between the hydrogels and background, fluorescent dyes were added to the hydrogel electric field receivers. (J) A SAER can detect human movements in real time. Scale bar, 25 cm. (K) The SAER successfully detects the movement of a person, even when a 3-cm-thick wooden wall is blocking between the person and a hydrogel electric field receiver. Error bars represent SD ($n = 3$). Photo Credit: Won Jun Song and Younghoon Lee, Seoul National University.

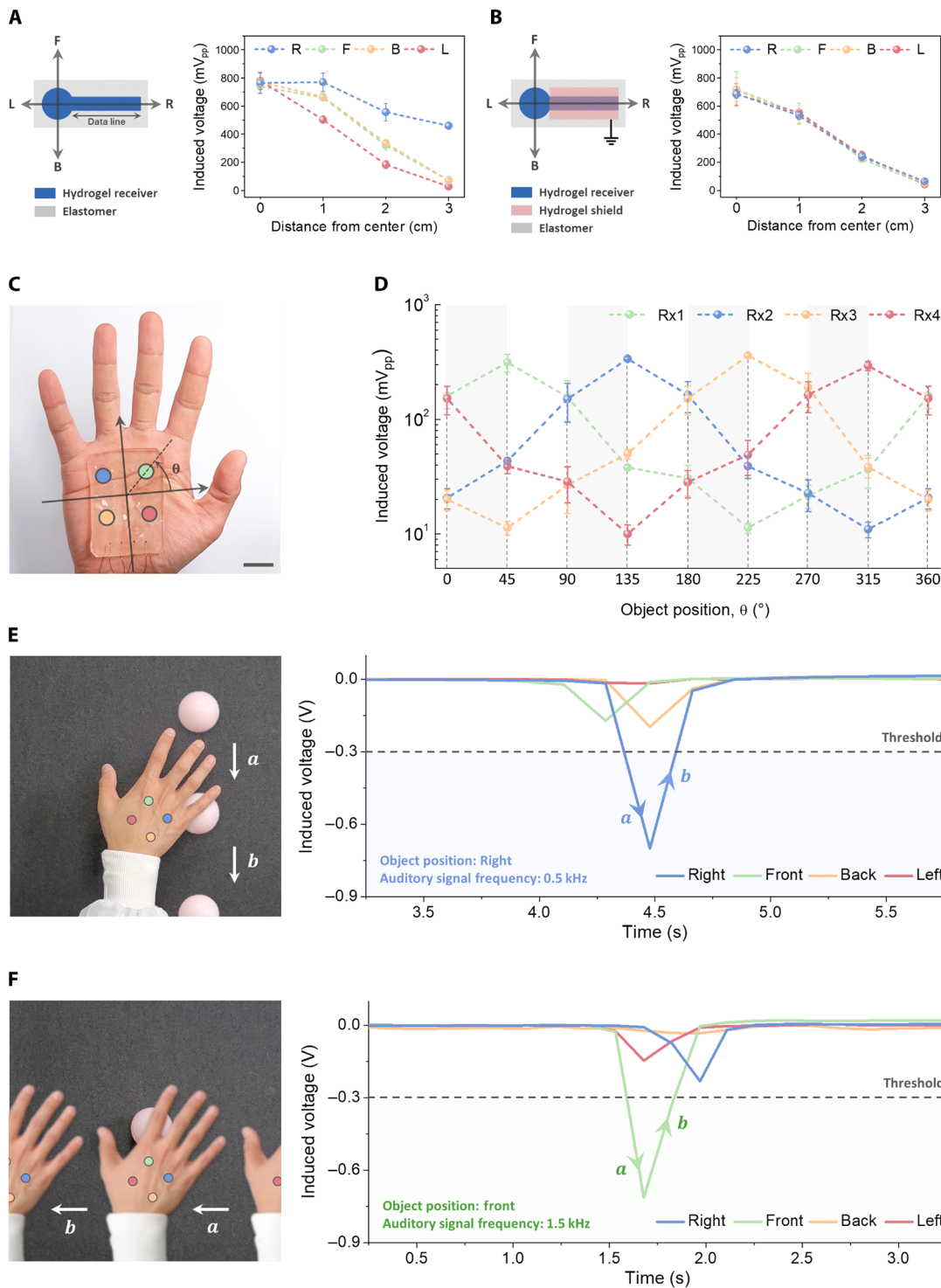


Fig. 6. A wearable SAER for noncontact spatial perception. (A) Without the conductive shield, data line connected to the receiver can cause distortion of the voltage signal. (B) When the data line is covered with a hydrogel conductive shield, the voltage signal from each electric field receiver became independent of the object direction. “L,” “R,” “F,” and “B” as “left,” “right,” “front,” and “back,” respectively. (C) The wearable SAER was attached to the hollow of the hand. Scale bar, 2 cm. (D) By comparing the intensity of the electric fields sensed by each hydrogel receiver (Rx), the SAER can be used to locate the relative position of the object. (E and F) By wearing the SAER, a person can perceive spatial information related to a dynamic (E) and static (F) object via auditory signals. Error bars represent SD ($n = 3$). Photo credit: Won Jun Song and Younghoon Lee, Seoul National University.

the relative position of their prey. By comparing the intensity of the electric fields sensed by each electroreceptor in the network, the animals can perceive the relative positions of their prey without making physical contact.

Similar to each individual electroreceptor of elasmobranch fishes, SAER with one electric field receiver can only measure the intensity and polarity of the electric field. Thus, while the artificial receptor can detect an object's approach, it cannot perceive the object's relative position. To introduce the capacity for noncontact object localization to the artificial receptor, we emulate the network structure of the animal's electroreceptor. Because the intensity of the electric field that reaches the receiver is a function of the relative distance between the object and the receiver, the relative position of the object can be estimated by comparing the amplitude of the induced voltages measured by each electric field receiver in the SAER.

To compare of the voltage signals measured by the network of electric field receivers, each receiver must be connected to a data line (Fig. 6A). However, even if the data lines are encapsulated with an elastomer, they can also act as an electric field receiver because the electric field can be transmitted through the dielectric materials. Undesirable transmission can cause distortion of the voltage signal by the data line. However, to accurately detect the relative position of an object by comparing the voltage signals from networks of electric field receivers, the voltage induction must be a function of only distance to the object, regardless of the object direction. Thus, the hydrogel conductive shield was used to prevent the object's electric field from reaching the data line (Fig. 6B). When the data line was covered by the conductive shield, the voltage signal from each electric field receiver became independent of the object direction.

To support human spatial perception in daily life, a wearable SAER was fabricated using a 3D printer (Fig. 6C). The SAER was composed of four different layers: a cover layer, two shielding layers, and a sensing layer (fig. S13). The sensing layer was composed of four hydrogel electric field receivers printed on the elastomer, and the shielding layers were composed of a hydrogel conductive shield printed on the elastomer. The sensing layer was sandwiched between the two shielding layers to accurately detect nearby objects. The bottom shielding layer blocks electrical noise from the subject's hand, and the top shielding layer prevents data lines from distorting the voltage signal. By comparing the amplitude of the voltage induced in each hydrogel electric field receiver, the SAER could locate the relative position of an object (Fig. 6D and fig. S14). In addition, the SAER with four hydrogel receivers could distinguish between eight relative object positions, and the addition of extra receivers to the sensing layer would potentially allow the SAER to identify more complex spatial information.

To characterize the wearability of the SAER, it was attached to the hollow of a subject's hand (Fig. 6C and movie S6). Because the SAER was composed of soft materials only, it could be deformed smoothly and comfortably with the skin. The robust hydrogel/elastomer interface allowed the SAER to withstand mechanical strain caused by hand movements without delamination. As the mechanical deformation leads to a negligible increase in the resistance of the hydrogel electric field receiver compared to that of the external load, the sensing capability of the SAER is not diminished by movement of the subject (fig. S15). In addition, high transparency enabled continuous inspection of the skin covered by the artificial receptor (23).

To support human spatial recognition, the wearable SAER was programmed to transmit spatial information of a nearby object via auditory signals (Fig. 6, E and F, and movie S6). Auditory signals with frequencies of 0.5, 1.0, 1.5, and 2 kHz corresponded to object positions of right, back, front, and left, respectively. The threshold voltage was set at 0.3 V to distinguish object-related signals from ambient noise. When the amplitudes of all voltage signals were below the threshold voltage, the SAER remained in the standby state. The SAER turned to the alert state when amplitude of the voltage signals exceeded the threshold voltage, and the auditory signal corresponding to the object's position was transmitted to the person wearing the receptor. Thus, by wearing the SAER, a person who is blind or visually impaired can recognize the relative positions of surrounding objects without any unwanted physical contact.

DISCUSSION

Inspired by how elasmobranch fishes locate their prey in a noncontact manner, we developed a SAER that emulate the ability to sense electric fields. As in the animal's electroreceptors, ion conductive hydrogels were used as soft electric field receivers. For rapid and elaborate fabrication, network of hydrogel electric field receivers was 3D printed on an elastomer. By covalently anchoring the hydrogels to the elastomer during the printing process, a robust hydrogel/elastomer interface capable of withstanding the mechanical deformation caused by human movement was formed. In the same manner as the electroreceptors of the elasmobranch fishes, the fabricated SAER could detect the relative position of nearby objects in a noncontact manner by comparing the intensity of the object-originated electric fields sensed by each hydrogel receiver in the network. Because electric fields can be transmitted through dielectric materials, the SAER could be used to detect objects even if they were behind a dielectric wall. Moreover, the sensing capability of the SAER was boosted more than 130-fold on the basis of the theoretical analysis. By wearing the SAER, a person can receive spatial information of a nearby object in real time via auditory signals. The artificial electroreceptor expands the way in which humans can perceive space by providing a new sensory modality that did not evolve naturally in human beings.

MATERIALS AND METHODS

Characterization of electroreception in rays

Electroreception in a ray (i.e., *P. motoro*) was observed in a tank with a size of 60 cm by 45 cm by 45 cm (length by width by height). An odor-delivery tube was placed in the center of the tank, and two electrodes were placed on either side of the tube (fig. S16). The whole experimental setup was disguised as buried under sand. A function generator (Agilent, 33612A) was used to supply an alternating current with the amplitude of 5 μ A and frequency of 2 Hz to the electrode, which simulated the electric field generated by the biomechanical activity of a prey animal (6). The prey-searching behavior of the ray was recorded using a video camera installed above the tank. The moving trajectory of the ray was obtained by locating the point at the center of the ray's two eyes over time and connecting the data points. The response of the ray to the electric field was quantitatively analyzed by measuring the duration the moving trajectory of the ray was located within 7.5 cm from the center of the electrode. All animal experiments were reviewed and

approved by the Institutional Animal Care and Use Committee of Seoul National University.

Materials and specimen preparation

SAERs were fabricated using a polyacrylamide hydrogel containing LiCl. Acrylamide (AAM; Merck, A8887) and *N,N*-methylenebisacrylamide (MBAAM; Merck, M7279) were used as a monomer and cross-linker for the hydrogel, respectively. LiCl (Merck, L4408) was used as an ionic charge carrier. Lithium phenyl-2,4,6-trimethylbenzoylphosphinate (LAP; Merck, 900889) and benzophenone (BP; Merck, B9300) were used as a photoinitiator and UV-assisted grafting agent, respectively. Very High Bond (VHB) tapes (3M, 4905) were used as elastomers in the SAERs.

Preparation of hydrogel precursor solution

A hydrogel precursor solution was prepared by dissolving AAM and LiCl in deionized water. The molar concentrations of the AAM and LiCl were both 2 M; 1.55 weight % (wt %) of MBAAM and 1.24 wt % of LAP with respect to the weight of AAM were added to the solution.

SAER fabrication process

The VHBs were immersed in BP solution (15 wt % in ethanol) for 10 min for swelling-driven absorption. Then, the VHBs were washed with ethanol and completely dried with nitrogen gas. The grafting agent-absorbed VHBs were treated with a 365-nm UV lamp (UVP, UVGL-25) for 10 s. Hydrogel electric field receivers with a diameter of 2 cm and a thickness of 200 μm were printed on the grafting agent-activated VHBs using a DLP 3D printer (Litho Advanced 3D printer, Illuminaid). During printing, the hydrogel precursor solution was exposed to 385-nm UV light for 10 s. After printing, the precursor solution on the surface of the fabricated hydrogel/elastomer hybrids was fully removed using nitrogen gas. To enhance the contrast between the hydrogels and elastomers, fluorescent dyes (Merck, R6626) were added to some of the hydrogels.

Mechanical testing

For uniaxial-tensile tests of the hydrogel/elastomer hybrids, a 200- μm -thick hydrogel was printed on the VHB. The test was carried out using a universal testing machine (Instron, 3343) with a receding rate of 1 cm/min.

Numerical analysis

The induced voltage across the external load, V , and theoretical capacitance between the object and the receiver, C_{FEM} , were computed by the FEM using COMSOL Multiphysics (see the Supplementary Materials for details). The built-in MATLAB routine integral was used to numerically compute Eq. 2 (see the Supplementary Materials for details).

Characterization of sensing capability

A hydrogel electric field receiver with a diameter of 2 cm and a thickness of 200 μm was connected to an external load of 5 gigohm. An electrometer (Keithley, 6517A) was used to measure the induced voltage across the external load. A pushing tester (Labworks, LW139.138-40), a linear power amplifier (Labworks, PA-138) and a function generator (Agilent, 33612A) were used to provide vertical simple harmonic oscillation of the objects (fig. S2). The initial distance, amplitude, and frequency of the oscillating object were 3 cm, 1 cm,

and 2 Hz, respectively. To prevent ambient electrical noise, measurements were conducted on a grounded metal table surrounded by a Faraday cage (see the Supplementary Materials and figs. S9 and S10). The PFA film was fixed on an acrylic substrate with a size of 30 mm by 30 mm by 5 mm (length by width by thickness), and this was used as the object. The object was charged by rubbing it with PP film.

Digital signal processing

The built-in MATLAB routines lowpass and highpass were used to reduce the noise in the voltage signal caused by the ambient dynamic object (see the Supplementary Materials for details).

Dehydration test

A hydrogel electric field receiver with a diameter of 2 cm and a thickness of 200 μm was encapsulated using VHB. The fabricated receiver was left in an environment with a temperature of 25°C and a humidity of 30%. Then, the weight, electrical resistance, and sensing capability of the hydrogel electric field receiver were measured over time. The weight of the receiver was measured using an analytical balance (Radwag, AS 82/220.R2). The electrical resistance of the receiver was measured using an LCR meter (Agilent, E4980A) with Ag/AgCl electrodes.

Characterization of through-wall sensing capability

To characterize the through-wall sensing capability of the SAER, dielectric barriers and hydrogel conductive shields were placed between the receivers and the object, respectively. The dielectric barriers were 50 mm by 50 mm by 15 mm (length by width by thickness) in size. The relative permittivities of the barrier materials were measured using an LCR meter (Agilent, E4980A) with dielectric constant measurement fixture (Keysight, 16451B) (table S1). The hydrogel conductive shield, 50 mm by 50 mm by 0.2 mm (length by width by thickness) in size, was fabricated using a 3D printer and connected to ground. To investigate the effect of the data line on the sensing capability, the receiver was connected to a data line with a size of 50 mm by 3 mm by 0.2 mm (length by width by thickness).

Demonstration of the through-wall sensing capability: Object movement

Two hydrogel electric field receivers with a size of 20 mm by 20 mm by 5 mm (length by width by thickness) were prepared. Both receivers were connected to the external load of 5 gigohm with indium tin oxide-coated polyethylene terephthalate film (Merck, 639303). LabView (National Instruments) was used to turn on LEDs when the induced voltage exceeded a threshold voltage. The distance between the pendulum and the receiver was 2 cm. To demonstrate the through-wall sensing capability of the SAER, a dielectric barrier and conductive shield were placed between the receiver and the pendulum. A 2-mm-thick piece of paper was used as the dielectric barrier, and a 2-mm-thick grounded aluminum sheet was used as the conductive shield.

Demonstration of the through-wall sensing capability: Human movement

The hydrogel electric field receiver with a size of 50 mm by 50 mm by 2 mm (length by width by thickness) was connected to an external load of 10 gigohm with silver-plated copper wire. The receiver was attached to a wooden wall with a size of 1770 mm by 1200 mm by

30 mm (length by width by thickness). The distance between the wall and the walking path of the person was approximately 30 cm.

Demonstration of a wearable SAER for spatial perception

The sensing and shielding layers of the wearable SAER were fabricated using the 3D printer. The thickness of the printed hydrogels in each layer was 200 μm . The sensing layer comprised four hydrogel electric field receivers with a diameter of 1 cm. The distance between adjacent receivers was 3 cm. The hydrogel conductive shield of the top shielding layer was designed to cover all data lines in the sensing layer. The hydrogel conductive shield of the bottom shielding layer was designed to cover all data lines and receivers in the sensing layer. The wearable SAER was assembled by sequentially stacking the bottom shielding layer, sensing layer, top shielding layer, and cover layer. Coaxial cables were used to connect the hydrogels of the SAER to the external loads and ground. LabView was used to generate auditory signals when a nearby object was detected. All procedures involving human subjects were reviewed and approved by the Institutional Review Board of Seoul National University. All subjects provided informed consent.

SUPPLEMENTARY MATERIALS

Supplementary material for this article is available at <https://science.org/doi/10.1126/sciadv.abg9203>

REFERENCES AND NOTES

- J. M. Loomis, R. L. Klatzky, Functional equivalence of spatial representations from vision, touch, and hearing: Relevance for sensory substitution. (2008).
- N. Qian, Binocular disparity and the perception of depth. *Neuron* **18**, 359–368 (1997).
- A. J. Kalmijn, Electric and magnetic field detection in elasmobranch fishes. *Science* **218**, 916–918 (1982).
- N. W. Bellono, D. B. Leitch, D. Julius, Molecular basis of ancestral vertebrate electroreception. *Nature* **543**, 391–396 (2017).
- B. Kramer, *Electroreception and Communication in Fishes* (Gustav Fischer, 1996), vol. 42.
- E. E. Josberger, P. Hassanzadeh, Y. Deng, J. Sohn, M. J. Rego, C. T. Amemiya, M. Rolandi, Proton conductivity in ampullae of Lorenzini jelly. *Sci. Adv.* **2**, e1600112 (2016).
- L. L. Harris, C. N. Bedore, S. M. Kajiura, Electroreception in the obligate freshwater stingray, *Potamotrygon motoro*. *Mar. Freshw. Res.* **66**, 1027–1036 (2015).
- T. Szabo, A. Kalmijn, P. Enger, T. H. Bullock, Microampullary organs and a submandibular sense organ in the fresh water ray, *potamotrygon*. *J. Comp. Physiol.* **79**, 15–27 (1972).
- T. Ha, J. Tran, S. Liu, H. Jang, H. Jeong, R. Mitbänder, H. Huh, Y. Qiu, J. Duong, R. L. Wang, A chest-laminated ultrathin and stretchable E-tattoo for the measurement of electrocardiogram, seismocardiogram, and cardiac time intervals. *Adv. Sci.* **6**, 1900290 (2019).
- H. Jeong, L. Wang, T. Ha, R. Mitbänder, X. Yang, Z. Dai, S. Qiao, L. Shen, N. Sun, N. Lu, Modular and reconfigurable wireless E-tattoos for personalized sensing. *Adv. Mater. Technol.* **4**, 1900117 (2019).
- G. Kettlgruber, D. Danninger, R. Moser, M. Drack, C. M. Siket, D. Wirthl, F. Hartmann, G. Mao, M. Kaltenbrunner, S. Bauer, Stretch-safe: Magnetic connectors for modular stretchable electronics. *Adv. Intell. Syst.* **2**, 2000065 (2020).
- C. Yang, Z. Suo, Hydrogel ionotronics. *Nat. Rev. Mater.* **3**, 125–142 (2018).
- H. R. Lee, C. C. Kim, J. Y. Sun, Stretchable Ionics—a promising candidate for upcoming wearable devices. *Adv. Mater.* **30**, 1704403 (2018).
- Y. Lee, W. Song, J.-Y. Sun, Hydrogel soft robotics. *Mater. Today Phys.* **15**, 100258 (2020).
- X. Liu, J. Liu, S. Lin, X. Zhao, Hydrogel machines. *Mater. Today* **36**, 102–124 (2020).
- J.-Y. Sun, X. Zhao, W. R. Illeperuma, O. Chaudhuri, K. H. Oh, D. J. Mooney, J. J. Vlassak, Z. Suo, Highly stretchable and tough hydrogels. *Nature* **489**, 133–136 (2012).
- C. Keplinger, J.-Y. Sun, C. C. Foo, P. Rothemund, G. M. Whitesides, Z. Suo, Stretchable, transparent, ionic conductors. *Science* **341**, 984–987 (2013).
- C. Larson, B. Peele, S. Li, S. Robinsom, M. Totaro, L. Beccai, B. Mazzolai, R. Shepherd, Highly stretchable electroluminescent skin for optical signaling and tactile sensing. *Science* **351**, 1071–1074 (2016).
- J. Odent, T. J. Wallin, W. Pan, K. Krueplestaedter, R. F. Shepherd, E. P. Giannelis, Highly elastic, transparent, and conductive 3D-printed ionic composite hydrogels. *Adv. Funct. Mater.* **27**, 1701807 (2017).
- F. Hartmann, M. Baumgartner, M. Kaltenbrunner, Becoming sustainable, the new frontier in soft robotics. *Adv. Mater.* **33**, 2004413 (2021).
- Y. Lee, W. J. Song, Y. Jung, H. Yoo, M.-Y. Kim, H.-Y. Kim, J.-Y. Sun, Ionic spiderwebs. *Sci. Robot.* **5**, eaaz5405 (2020).
- Y. Lee, S. H. Cha, Y.-W. Kim, D. Choi, J.-Y. Sun, Transparent and attachable ionic communicators based on self-cleanable triboelectric nanogenerators. *Nat. Commun.* **9**, 1804 (2018).
- J. Y. Sun, C. Keplinger, G. M. Whitesides, Z. Suo, Ionic skin. *Adv. Mater.* **26**, 7608–7614 (2014).
- C.-C. Kim, H.-H. Lee, K. H. Oh, J.-Y. Sun, Highly stretchable, transparent ionic touch panel. *Science* **353**, 682–687 (2016).
- H. Yuk, T. Zhang, G. A. Parada, X. Liu, X. Zhao, Skin-inspired hydrogel–elastomer hybrids with robust interfaces and functional microstructures. *Nat. Commun.* **7**, 12028 (2016).
- Q. Liu, G. Nian, C. Yang, S. Qu, Z. Suo, Bonding dissimilar polymer networks in various manufacturing processes. *Nat. Commun.* **9**, 846 (2018).
- P. Le Floch, X. Yao, Q. Liu, Z. Wang, G. Nian, Y. Sun, L. Jia, Z. Suo, Wearable and washable conductors for active textiles. *ACS Appl. Mater. Interfaces* **9**, 25542–25552 (2017).
- J. Yang, R. Bai, B. Chen, Z. Suo, Hydrogel adhesion: A supramolecular synergy of chemistry, topology, and mechanics. *Adv. Funct. Mater.* **30**, 1901693 (2020).
- D. Wirthl, R. Pichler, M. Drack, G. Kettlgruber, R. Moser, R. Gerstmayr, F. Hartmann, E. Bradt, R. Kaltseis, C. M. Siket, Instant tough bonding of hydrogels for soft machines and electronics. *Sci. Adv.* **3**, e1700053 (2017).
- H. Baytekin, A. Patashinski, M. Branicki, B. Baytekin, S. Soh, B. A. Grzybowski, The mosaic of surface charge in contact electrification. *Science* **333**, 308–312 (2011).
- D. Clarke, H. Whitney, G. Sutton, D. Robert, Detection and learning of floral electric fields by bumblebees. *Science* **340**, 66–69 (2013).
- H. H. Zakon, Electric fields of flowers stimulate the sensory hairs of bumble bees. *Proc. Natl. Acad. Sci.* **113**, 7020–7021 (2016).
- C.-C. Kim, Y. Kim, S.-H. Jeong, K. H. Oh, K. T. Nam, J.-Y. Sun, An implantable ionic wireless power transfer system facilitating electrosynthesis. *ACS Nano* **14**, 11743–11752 (2020).
- D. J. Griffiths. (American Association of Physics Teachers, 2005).
- W. Seung, H. J. Yoon, T. Y. Kim, H. Ryu, J. Kim, J. H. Lee, J. H. Lee, S. Kim, Y. K. Park, Y. J. Park, Boosting power-generating performance of triboelectric nanogenerators via artificial control of ferroelectric polarization and dielectric properties. *Adv. Energy Mater.* **7**, 1600988 (2017).
- Z. L. Wang, Triboelectric nanogenerators as new energy technology for self-powered systems and as active mechanical and chemical sensors. *ACS Nano* **7**, 9533–9557 (2013).
- M. M. Emara, D.-E. A. Mansour, A. M. Azmy, in *2015 4th International Conference on Electric Power and Energy Conversion Systems (EPECS)* (IEEE, 2015), pp. 1–5.

Acknowledgments

Funding: This work was supported by National Research Foundation of Korea (NRF) grants funded by the Korean government (no. 2018M3A7B4089670, 2018R1A3B1052541, 2015R1A5A1037668, 2018-052541, 2017M3D9A1073922, and 2021R1C1C2009703), by ITECH R&D program of MOTIE/KEIT (project no. 20001240), and by the Materials and Components Technology Development Program of MOTIE/KEIT (10052783). H.-Y.K. acknowledges administrative support from SNU-IAMD. **Author contributions:** W.J.S. and Y.L. conceived of the idea, carried out the experiments, and wrote the main manuscript. W.J.S., Y.L., and J.-M.P. contributed to the data analysis. W.J.S. and Y.-W.K. fabricated the device. Y.J. and H.-Y.K. developed the mathematical model and wrote the manuscript. J.K. and Y.-L.P. developed the program that enabled interaction between the fabricated device and computer. J.-Y.S. supervised this study and provided intellectual and technical guidance. All authors discussed the results and commented on the manuscript. **Competing interests:** The authors declare that they have no competing interests. **Data and materials availability:** All data needed to evaluate the conclusions in the paper are present in the paper and/or the Supplementary Materials.

Submitted 5 February 2021

Accepted 7 October 2021

Published 24 November 2021

10.1126/sciadv.abg9203